Efficient high-fidelity flying qubit shaping

Benedikt Tissot ●* and Guido Burkard ●†

Department of Physics, University of Konstanz, D-78457 Konstanz, Germany

Matter qubit to traveling photonic qubit conversion is the cornerstone of numerous quantum technologies such as distributed quantum computing, as well as several quantum internet and networking protocols. We formulate a theory for stimulated Raman emission which is applicable to a wide range of physical systems, including quantum dots, solid-state defects, and trapped ions, as well as various parameter regimes. We find the upper bound for the photonic pulse emission efficiency of arbitrary matter qubit states for imperfect emitters and show a path forward to optimizing the fidelity. Based on these results, we propose a paradigm shift from optimizing the drive to directly optimizing the temporal mode of the flying qubit using a closed-form expression. Protocols for the production of time-bin encoding and spin-photon entanglement are proposed. Furthermore, the mathematical idea to use input-output theory for pulses to absorb the dominant emission process into the coherent dynamics, followed by a non-Hermitian Schrödinger equation approach, has great potential for studying other physical systems.

I. INTRODUCTION

Efficient, tunable, and coherent quantum emitters are at the heart of many quantum technologies. Prominent examples include entanglement distribution [1,2], as well as more general applications for quantum networks and communication [3–8], which can potentially enable a quantum internet [9,10] with quantum-mechanically enhanced security and privacy. Additionally, single-photon emission represents a cornerstone for several photonic technologies [11–15]. Generally, there is great interest in coherent quantum media conversion, as it allows the connection between different quantum systems with diverse properties. This enables hybrid quantum systems that combine the advantages of each subsystem. Such hybrid quantum systems can combine matter systems with beneficial properties for storage or computation, e.g., trapped ions [16], semiconductor qubits [17] implemented via quantum dots and defects in solids, and superconducting circuits [18], with easily transmittable photons [14]. In this regard, photons are the natural choice for traveling qubits [19] and can be used to exchange quantum states or create entanglement between distant matter systems.

Cavity-enhanced stimulated Raman emission is an established technique for controlled and (nearly) deterministic pulse emission, i.e., "push-button-like" shaped pulse generation. On-demand emission promises a leap towards the independence of emission and absorption, which is of the utmost importance when exchanging states between diverse systems. The ability of Purcell enhancement to achieve a controllable emitter with high efficiency was already shown over a wide range of materials, e.g., trapped ions as well as atoms [20–22], "untrapped" atoms [23], quantum dots [24,25], and defects in solids [26,27]. Previous theoretical work focused on perfect emitters [1,28–32].

In this paper we theoretically determine the fundamental fidelity bound of coherent state transfer for arbitrary pulse shapes from a stationary matter three-level system (3LS) via a cavity to a traveling qubit pulse which facilitates a distinct approach to maximize the state transfer fidelity. In particular, we are interested in the transfer of a superposition of *qubit states* $\alpha_0 |1\rangle + \beta_0 |0\rangle$ via the excited state $|e\rangle$ and cavity to the traveling photon (qubit) $\alpha_0 |1\rangle_v + \beta_0 |0\rangle_v$ (see Fig. 1).

Previously derived photon retrieval bounds [22,29,30,33] depending only on the cavity decay rate and cooperativity of the emitter-cavity coupling can greatly overestimate the bound we calculate, which includes additional system features, most prominently different decoherence processes of the emitter as well as the *temporal shape of the flying qubit* $v(t)$ and initial superposition states, which are fundamentally necessary to understand spin-photon entanglement. Because the bound depends on the shape of the photon, it is suited for finding optimized flying qubit shapes, providing a paradigm shift from approaches that aim to find the optimal drive, e.g., the shortcut to adiabaticity [34] approach as well as theories eliminating the propagating pulse completely [1]. The remainder of this paper is organized as follows. First, we show how stimulated Raman emission can be used to generate spin-photon entanglement in Sec. II. In Sec. III we introduce the model describing the emitter and the quantum pulse. We present a closed-form solution of the dynamics in Sec. IV and introduce the temporal mode matching (Sec. IV A) to link the emitter dynamics to the temporal mode. We use the solution to bound the state transfer fidelity

*benedikt.tissot@uni-konstanz.de
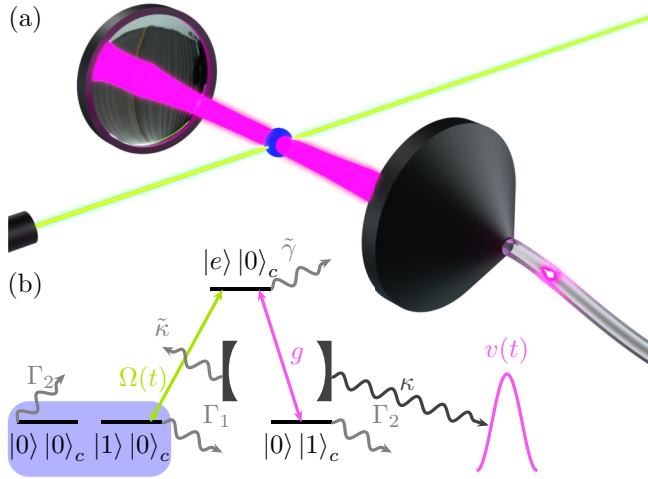†guido.burkard@uni-konstanz.de

FIG. 1. (a) Illustration of the physical system and (b) energy level diagram of a stimulated Raman emitter. The illustration depicts a quantum system (blue ball) coupled to an electromagnetic cavity mode (pink) as well as an excitation (e.g., laser) field (green). One of the mirrors couples out into a fiber, enabling the emission of a photon pulse (pink glowing droplet). The level diagram in (b) in the rotating frame depicts the excited state $|e\rangle$ (ES) split from the two ground states $|0\rangle$ and $|1\rangle$ by the detuning Δ for the relevant states of the cavity $|0\rangle_c$ and $|1\rangle_c$ with zero and one photon. The Λ system is set up by a controllable time-dependent (excitation field) Rabi amplitude $\Omega(t)$ coupling $|1\rangle|0\rangle_c$ to the ES, as well as cavity interaction between the ES and $|0\rangle|1\rangle_c$ with single-photon coupling strength g. The cavity emits the photon wave packet with pulse shape $v(t)$ via the (right) out-coupling κ, thus converting the matter qubit (shaded blue) to a flying qubit. Imperfections of the three-level system and cavity can lead to decoherence processes taken into account via the combined rates $\tilde{\gamma}$, Γ_1, Γ_2, and $\tilde{\kappa}$.

in Sec. IV B and show how to optimize the pulse shape to increase the fidelity in Sec. IV C. We conclude the paper in Sec. V.

II. ENTANGLEMENT GENERATION VIA STIMULATED RAMAN EMISSION

Prior to the detailed analysis we point out quantum technological applications of stimulated Raman emission beyond single-photon sources, e.g., to create a photon entangled with the matter qubit or to transfer the matter qubit to a time-bin qubit if an additional long-lived matter state or (nuclear) spin n is available. For concreteness, we focus on the silicon-vacancy center in diamond, an established Raman emitter [26,27] which features the silicon nuclear spin as a quantum memory. Recently, a C_nNOT gate between the electronic qubit and the nuclear spin was demonstrated using microwaves (fidelity $\sim$99.9%) [35]. After initializing the nuclear spin $\alpha_0 |1\rangle_n + \beta_0 |0\rangle_n$ state, we propose to use a nuclear C_nNOT followed by a Raman emission, resulting in the entangled state $\alpha_0 |1\rangle_n |1\rangle_v + \beta_0 |0\rangle_n |0\rangle_v$. The basic idea is to store the wave function amplitude β_0 (of the qubit state $|0\rangle$) in an ancillary state during the emission from the qubit state $|1\rangle$ to the first time bin $|1\rangle_1$.

After the first emission, gates are applied between the qubit and the ancillary state(s) so that after another emission the qubit state is encoded in two time bins, i.e., a time-bin qubit with the state $\alpha_0 |1\rangle_1 + \beta_0 |1\rangle_2$. The indices mark the time bins, which are independent pulses, e.g., pulses with nonoverlapping envelopes. In Fig. 2 we show two examples of the implementation of this idea, one for an ancillary qubit (as is the case for the silicon nuclear spin in the SiV) and one for a single ancillary state. For ancillary qubit implementation we need the two-qubit gates C_nNOT and SWAP, while for the single extra state $|a\rangle$ we need the ability to apply a $\pi/2$ rotation between $|0\rangle$ and $|a\rangle$; in both cases an X gate between $|0\rangle$ and $|1\rangle$ is also required. The EMIT gate corresponds to the stimulated Raman emission process. In both cases, stopping the protocol after the first emission or replacing the SWAP by another C_nNOT can be used to generate entanglement. For the single ancillary state the time-bin entanglement can be achieved by omitting the second $\pi/2$ pulse for the single ancillary state.

The entangled state after the first emission is $\alpha_0 |1\rangle_n |1\rangle_1 + \beta_0 |0\rangle_n |0\rangle_1$ using the ancillary qubit with states $|\sigma\rangle_n$ ($\sigma = 0, 1$) or $\alpha_0 |0\rangle |1\rangle_1 + \beta_0 |a\rangle |0\rangle_1$ using only one ancillary state $|a\rangle$, where $|m\rangle_1$, with $m = 0, 1, \ldots$, is the number state of the first emitted pulse. For the time-bin entanglement we find $\alpha_0 |1\rangle_n |1\rangle_1 + \beta_0 |0\rangle_n |1\rangle_2$ and $\alpha_0 |a\rangle |1\rangle_1 + \beta_0 |0\rangle |1\rangle_2$. Analogously, initializing the system in one of the ancillary states and then repeating a (partial) transfer of the occupation to $|1\rangle$ followed by an emission enables time-bin qudit generation.

Applications for the protocol generating entanglement between a quantum memory and a flying qubit include entanglement exchange between distant matter nodes (heralded [36] or combined with perfect absorption [30,37] to "pitch and catch" [1]) and the generation of photonic cluster states [38]. Note that the following analysis is compatible with the outlined entanglement generation protocols because the analytical solution makes assumptions about only the initial preparation of the Raman emitter.

III. MODEL

In this scenario the quantum memory is better shielded from decoherence than the emitter, making it vital to understand and optimize the emission. The rotating frame Hamiltonian (see Appendix A for additional details on the rotating frame) of the cavity interacting with the 3LS is

$$H_S/\hbar = \Delta |e\rangle \langle e| + [\Omega(t) |e\rangle \langle 1| + gc^\dagger |0\rangle \langle e| + \text{H.c.}], \quad (1)$$

with $\Omega(t)$ being the time-dependent Rabi frequency of the drive; g being the single-photon coupling strength to the cavity; Δ being the detuning between the cavity and the $|0\rangle \leftrightarrow |e\rangle$ transition; $|0\rangle, |1\rangle$, and $|e\rangle$ being the 3LS states; and c being the cavity photon annihilation operator. The energy level structure is sketched in Fig. 1.

To include the emission from the cavity in a specific output pulse in the Hermitian dynamics we employ the recently developed input-output theory for quantum pulses [39,40] using an open quantum systems approach. Therefore, we can use dissipators L_i to model various incoherent processes and rely on the Born-Markov approximation. Since the relevant

(a)

$$|1\rangle_n |0\rangle \xrightarrow{\text{C}_n\text{NOT}} |1\rangle_n |1\rangle \xrightarrow{\text{EMIT}} |1\rangle_n |0\rangle |1\rangle_1 \xrightarrow{\text{SWAP}} |0\rangle_n |1\rangle |1\rangle_1 \xrightarrow{X} |0\rangle_n |0\rangle |1\rangle_1 \xrightarrow{\text{EMIT}} |0\rangle_n |0\rangle |1\rangle_1$$

$$|0\rangle_n |0\rangle \longrightarrow |0\rangle_n |0\rangle \longrightarrow |0\rangle_n |0\rangle \longrightarrow |0\rangle_n |0\rangle \longrightarrow |0\rangle_n |1\rangle \longrightarrow |0\rangle_n |0\rangle |1\rangle_2$$

(b)

$$|1\rangle \xrightarrow{|0\rangle \overset{\pi/2}{\leftrightarrow} |a\rangle} |1\rangle \xrightarrow{\text{EMIT}} |0\rangle |1\rangle_1 \xrightarrow{|0\rangle \overset{\pi/2}{\leftrightarrow} |a\rangle} |a\rangle |1\rangle_1 \xrightarrow{X} |a\rangle |1\rangle_1 \xrightarrow{|0\rangle \overset{\pi/2}{\leftrightarrow} |a\rangle} |0\rangle |1\rangle_1 \xrightarrow{\text{EMIT}} |0\rangle |1\rangle_1$$

$$|0\rangle \longrightarrow |a\rangle \longrightarrow |a\rangle \longrightarrow |0\rangle \longrightarrow |1\rangle \longrightarrow |1\rangle \longrightarrow |0\rangle |1\rangle_2$$
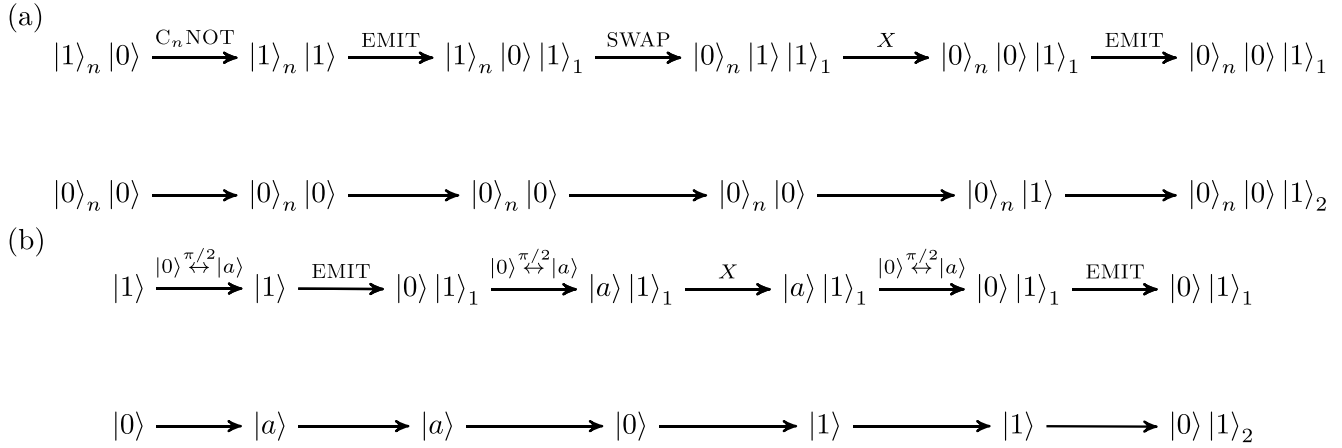
FIG. 2. Emission of a time-bin qubit using (a) an ancillary (e.g., nuclear spin) qubit or (b) an ancillary state. The main focus of this paper is the particular implementation of the EMIT process via cavity-enhanced stimulated Raman emission. C$_n$NOT and SWAP refer to the two qubit gates between the matter qubit and the ancillary qubit, and X denotes the one-qubit X gate of the matter qubit (or a $\pi/2$ pulse between $|0\rangle$ and $|1\rangle$). Additionally, if one implements the protocol only up to the first emission, matter-photon entanglement is achieved.

emission is into a pulse that travels away from the emitter, this approximation is justified provided the cavity coupling κ is approximately constant for the spectrum of the pulse and the emitted pulse varies slowly compared to the spectral range of the continuum field [40]. For a pulse with a carrier frequency in the optical range and durations on the order of 0.1 ns or a microwave pulse and durations down to 10 ns, we deem the assumptions well justified.

We take the input to be in the vacuum state and employ input-output theory for pulses [39,40] to model the emission (caused by directional single-photon losses c with rate κ) to the specific pulse as a *virtual cavity* with time-dependent coupling to the system. In this way, the cavity would completely absorb the specific pulse. This is achieved by a total Hamiltonian $H = H_S + \hbar \frac{i}{2}\sqrt{\kappa}[g_v^*(t)c^\dagger a - \text{H.c.}]$, where κ is the cavity decay rate, a is the annihilation operator of the virtual cavity, and $g_v(t) = -v^*(t)/\sqrt{\int_0^t dt'\,|v(t')|^2}$ is the time-dependent coupling strength, which is directly linked to the normalized pulse form $v(t)$, i.e., $\int_0^T |v(\tau)|^2\,d\tau = 1$, with T being the pulse duration. Combined with the dissipator $L_0(t) = g_v(t)^*a + \sqrt{\kappa}c$, the total Hamiltonian leads to a cascaded evolution, resulting in a transfer of the quantum amplitudes from the emitter to the virtual cavity. Additionally, a pulse shape that does not (perfectly) capture the dynamics of the emission process leads to incoherent losses via $L_0(t)$; in other words, only the emission into modes other than the temporal mode $v(t)$ are treated as losses.

To study the coherent state transfer of a matter state into the propagating wave packet, we focus on the single-excitation subspace using a non-Hermitian Hamiltonian approach [41–44], described by the time-dependent Schrödinger equation $i\hbar \frac{\partial}{\partial t}|\Psi\rangle = H_{\text{NH}}|\Psi\rangle$, with $H_{\text{NH}} = H - \hbar \frac{i}{2}\sum_i L_i^\dagger L_i$ and using the ansatz wave function

$$|\Psi(t)\rangle = [\alpha(t)|1\rangle + \beta(t)|0\rangle + i\zeta(t)|e\rangle]\,|0\rangle_c |0\rangle_v$$
$$+ \eta(t)|0\rangle|1\rangle_c|0\rangle_v + \lambda(t)|0\rangle|0\rangle_c|1\rangle_v. \quad (2)$$

IV. RESULTS

In the following we summarize the solution of the dynamics of the state transfer from the normalized state $|\Psi(0)\rangle = (\alpha_0|1\rangle + \beta_0|0\rangle)|0\rangle_c|0\rangle_v$ to a state close to $|\Psi_{\text{target}}\rangle = |0\rangle|0\rangle_c(\alpha_0|1\rangle_v + \beta_0|0\rangle_v)$. Our first objective is to find a (closed-form) expression for the (approximate) fidelity of the state transfer

$$F = |\langle\Psi(T)|\Psi_{\text{target}}\rangle|^2 = |\alpha_0^*\lambda(T) + \beta_0^*\beta(T)|^2 \quad (3)$$

as a function of the system parameters and the pulse shape. One of the distinguishing features of our method is that it does not require the repeated numerical solution of any differential equations.

A. Temporal mode matching

First, we solve the amplitude that does not partake in the emission and therefore is subject to only decoherence, $\beta(t) = \beta_0 e^{-\Gamma_2 t/2}$. Then we determine the optimal relationship between the wave function amplitudes [Eq. (2)] and the pulse shape by solving $L_0(t)|\Psi(t)\rangle = 0$ for the time-dependent coupling $g_v(t)$ to the virtual cavity. Fulfillment of this condition implies that the successful coherent emission is a no-jump trajectory in the model and yields

$$g_v(t) = -\sqrt{\kappa}\eta^*(t)/\lambda^*(t), \quad (4)$$

which corresponds to the *temporal mode matching* condition. While the ideal process is fully coherent in our model, the remaining incoherent processes (L_i, $i \neq 0$) describe unwanted errors. Thus, we have immediate access to the probability of these errors $p_e = 1 - \langle\Psi(t)|\Psi(t)\rangle \geqslant 0$ via the loss of the wave function norm, underlining that the chosen approach is perfectly suited to describing the coherent transfer of population. Within p_e we here consider the combined decoherence rates $\tilde{\gamma}$, Γ_1, and Γ_2 for the 3LS states $|e\rangle$, $|1\rangle$, and $|0\rangle$, respectively, as well as additional losses of the cavity $\tilde{\kappa}$. In Appendix B we relate the combined decoherence rates to the corresponding dissipators of the Lindblad

master equation modeling incoherent transitions, e.g., decay and dephasing processes. We focus on efficient quantum emitters where high fidelities are possible. By employing the Cauchy-Schwartz inequality we find $p_e \leqslant 1 - F$ such that p_e is small ($p_e \ll 1$) for suitable pulses that reach high fidelities. This makes our approach highly accurate because the unwanted emission of multiple excitations and the back-action on the coherent trajectory after a quantum jump that are neglected within the non-Hermitian Schrödinger equation are highly unlikely. This confirms the usefulness of the non-normalized coherent trajectory to calculate fidelities approaching unity.

The pulse shape can be linked to the dynamics via the temporal mode matching (4). Combining the mode matching condition (4) with the non-Hermitian Schrödinger equation, we arrive at a set of differential equations for the amplitudes, whose solution we calculate in Appendix C. We find

$$\eta(t) = E\alpha_0 e^{-\Gamma_2 t/2} v(t)/\sqrt{\kappa}, \tag{5}$$

$$\lambda(t) = E\alpha_0 e^{-\Gamma_2 t/2} \sqrt{\int_0^t |v(\tau)|^2 \, d\tau}, \tag{6}$$

where the positive proportionality constant E takes into account that the pulse shape is normalized independently of the dynamics; we term it *matter-photon (amplitude) conversion efficiency* since it can be defined as the (renormalized) amplitude transfer ratio $E = [\lambda(T)/\alpha_0]e^{\Gamma_2 T/2}$. In turn, the fidelity (3) is directly bound by $\alpha_0^* \lambda(T)$ and thus by the maximal achievable $E_{\max}$. To calculate $E_{\max}$, we apply the idea of photon shaping [31], where we solve the non-Hermitian dynamics in reverse by imposing η and λ, resulting in

$$\zeta(t) = \frac{\Gamma_2 + \kappa + \tilde{\kappa}}{2g}\eta(t) + \frac{1}{g}\dot{\eta}(t), \tag{7}$$

$$\Omega(t) = -\frac{(\tilde{\gamma}/2 + i\Delta)\zeta(t) + g\eta(t) + \dot{\zeta}(t)}{\alpha(t)}. \tag{8}$$

The remaining amplitude evolves according to

$$\alpha(t) = \alpha_0 e^{i\phi(t) - \Gamma_1 t/2}\sqrt{1 - E^2 \int_0^t d(\tau)d\tau}, \tag{9}$$

with the phase evolution $\phi(t)$ and the (renormalized) depletion rate $d(t)$, which are closed-form analytic functions of the pulse shape $v(t)$ and system parameters $g, \kappa, \tilde{\gamma}, \tilde{\kappa}, \Gamma_1$, and Γ_2. The depletion rate is

$$d(t) = e^{t(\Gamma_1 - \Gamma_2)}\left(\left\{1 + \frac{\tilde{\kappa}}{\kappa} + \frac{\tilde{\gamma} - \Gamma_2}{g^2}\left[\frac{\kappa}{4}\left(1 + \frac{\tilde{\kappa}}{\kappa}\right)^2 + \frac{\dot{\theta}^2(t)}{\kappa}\right] + \frac{2\ddot{\theta}(t)\dot{\theta}(t)}{\kappa g^2}\right\}f^2(t) + \frac{1}{g^2}\left(1 + \frac{\tilde{\kappa}}{\kappa}\right)f(t)\ddot{f}(t) + \frac{2}{\kappa g^2}\dot{f}(t)\ddot{f}(t)\right.$$

$$\left. + \left[\frac{2}{\kappa} + \frac{\kappa}{2g^2}\left(1 + \frac{\tilde{\kappa}}{\kappa}\right)^2 + \frac{\tilde{\gamma} - \Gamma_2}{g^2}\left(1 + \frac{\tilde{\kappa}}{\kappa}\right) + \frac{2\dot{\theta}^2(t)}{\kappa g^2}\right]f(t)\dot{f}(t) + \left[\frac{1}{g^2}\left(1 + \frac{\tilde{\kappa}}{\kappa}\right) + \frac{\tilde{\gamma} - \Gamma_2}{\kappa g^2}\right]\dot{f}^2(t)\right), \tag{10}$$

where we introduce the photon envelope phase $\theta(t) \in \mathbb{R}$ and amplitude $f(t) \in \mathbb{R}$, i.e., $v(t) = e^{i\theta(t)}f(t)$. The phase evolution $\phi(t)$ can be found in Appendix C. We stress that $d(t)$ is independent of the detuning Δ and matter-photon conversion efficiency E. On the other hand, the phase evolution $\phi(t)$ is an integral expression additionally depending on Δ. For a pulse with constant complex phase and for $\Delta = 0$ we have $\phi(t) = 0$. We highlight that $\Omega(t), d(t)$, and $\phi(t)$ are all independent of the initial state of the matter qubit (α_0, β_0).

B. State transfer fidelity bound

A complex square root in Eq. (9) would contradict our ansatz such that we would find the bound

$$E \leqslant E_{\max} = \frac{1}{\sqrt{\max_{t \geqslant 0} \int_0^t d(\tau)d\tau}}. \tag{11}$$

Because as soon as the square root in Eq. (9) tends to zero the Rabi amplitude $\Omega(t)$ (8) diverges [unless $\eta(t), \zeta(t)$, and $\dot{\zeta}(t)$ vanish at the same time], the physical bound can be formulated even stronger such that the inequality becomes strict ($\leqslant \rightarrow <$) ensuring $|\alpha(t)| > 0$. The form of $d(\tau)$ [Eq. (10)] and Eq. (11) imply that a varying phase in the rotating frame, $\dot{\theta}(t) \neq 0$, is detrimental, i.e., reduces $E_{\max}$, if the phase of $|1\rangle$ can be controlled better than the ES ($\Gamma_1 < \tilde{\gamma}$). Using the method of partial

integration, $2\int_0^t e^{(\Gamma_1 - \Gamma_2)t}[\dot{\theta}\ddot{\theta}f^2 + \dot{\theta}^2 f\dot{f}]^2 dt = e^{(\Gamma_1 - \Gamma_2)t}f^2(t)\dot{\theta}^2(t) - (\Gamma_1 - \Gamma_2)\int_0^t \dot{\theta}^2 f^2 e^{(\Gamma_1 - \Gamma_2)t}dt$, when integrating Eq. (10) proves that a varying phase in the rotating frame reduces $E_{\max}$, as long as $\Gamma_1 < \tilde{\gamma}$. The bound on the parameter E also limits the fidelity (3),

$$F \leqslant e^{-\Gamma_2 T}\left|1 - (1 - E_{\max})|\alpha_0|^2\right|^2. \tag{12}$$

The fraction of the amplitude transferred from $|1\rangle$ to $|1\rangle_v$ corresponds to the worst-case fidelity $F(|\alpha_0| = 1) = |\lambda(T)/\alpha_0|^2 = E^2 e^{-\Gamma_2 T} \leqslant E_{\max}^2 e^{-\Gamma_2 T}$ and does not depend on the initial condition. This result is a generalization of the upper bound for the maximum efficiency in Ref. [31], and we emphasize that by incorporating the imperfections of the emitter the fidelity has a maximum at a finite time (see Fig. 3) and is therefore suited to optimize the pulse duration. Considering that any initial matter-qubit state should be transferred with a good fidelity, we average the fidelity (12) over the Bloch sphere

$$F_{\text{avg}} = \frac{E^2 + E + 1}{3e^{\Gamma_2 T}} \leqslant \frac{E_{\max}^2 + E_{\max} + 1}{3e^{\Gamma_2 T}}. \tag{13}$$

To compare our result to previous bounds for perfect emitters ($\Gamma_1, \Gamma_2 = 0$) and slowly evolving pulses we first use $\max_t \int_0^t d(\tau)d\tau \geqslant \int_0^T d(\tau)d\tau$ and $\int_0^T d(\tau)d\tau > 0$ for good quantum emitters, where $\Gamma_1, \Gamma_2 < \kappa, \tilde{\gamma}$, employing
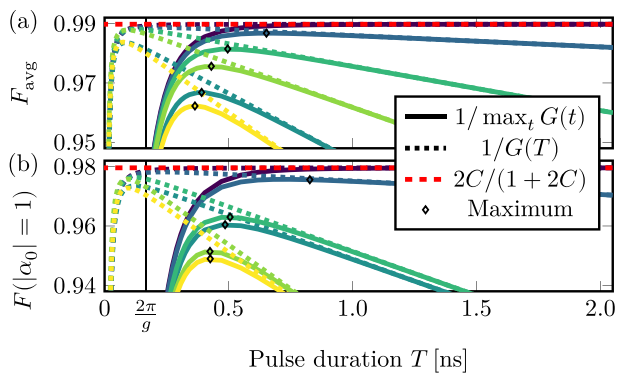
FIG. 3. Bounds for the (a) average and (b) worst-case fidelity as a function of the pulse duration for a $\sin^2$ pulse [see Eqs. (12) and (13)]. We compare different bounds, derived from different expressions for E^2 (see legend), the pulse form dependent fidelities based on the exact maximum (11) (solid lines), the simplified analytic bound $E^2 = 1/\int_0^T d(\tau)d\tau$ (dotted lines), and the approximation for slowly varying pulses and perfect emitters $E^2 = 2C/(1 + 2C)$ [see Eq. (14); dashed line]. The maxima of the fidelity based on the exact maximum are marked by diamonds. The pulse form dependent bounds are shown for different decoherences of the matter qubit $(\Gamma_1, \Gamma_2)/\tilde{\gamma}$; from dark (blue) to light (yellow) the values are $(0,0)$, $(0.01,0.005)$, $(0,0.1)$, $(0.1,0)$, $(0.2,0)$, and $(0.1,0.1)$. We use cavity QED parameters that can describe silicon-vacancy defects in diamond $(g, \kappa, \gamma) = 2\pi \times (6, 30, 0.1)$ GHz inside a perfect one-sided cavity $\tilde{\kappa} = 0$.

$\int_0^T d(\tau)d\tau$ as a "simpler" upper bound for Eqs. (11)–(13). In Fig. 4 we show $\exp(\Gamma_2 T)\int_0^T d(\tau)d\tau$ for $\sin^2$ pulses of different durations and for different decoherence rates of the emitter. Figure 4 shows that for long pulse durations the difference between $\int_0^T d(\tau)d\tau$ and $\max_t \int_0^t d(\tau)d\tau$ becomes smaller. It is also readily visible that for short pulses the maximum deviates from $\int_0^T d(\tau)d\tau$. We can further approximate this for a slowly evolving pulse $\dot{v} \ll \kappa, g$ and perfect emitter to

$$E^2 \lesssim \frac{\kappa}{\kappa + \tilde{\kappa}}\frac{2C}{(1 + 2C)}, \qquad (14)$$

with $C = 2g^2/[\tilde{\gamma}(\kappa + \tilde{\kappa})]$ being the (generalized) cooperativity. This is in agreement with the photon escape (or retrieval) efficiency found in [22,29,30,33].
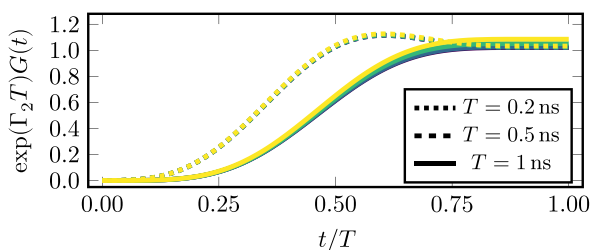

FIG. 4. Integrated depletion rate $\int_0^t d(\tau)d\tau$ [see Eq. (10)] for a $\sin^2$ pulse as a function of integration time t. We use this integral to calculate the maximum achievable fidelity for a set of parameters. Here, we consider a $\sin^2$ pulse which corresponds to the ansatz in Eq. (15) with $L = 1$. We use the same colors and parameters as in Fig. 3.
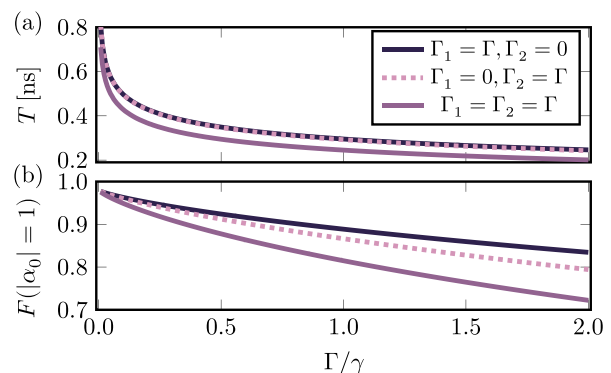

FIG. 5. Optimal pulse duration T for $L = 1$ and worst-case fidelity $F(|\alpha_0| = 1) = |\lambda(T)/\alpha_0|^2$ as a function of the matter qubit decoherence rates Γ_1 and Γ_2 (see legend). The colors correspond to different decoherence processes (see legend). We use the same parameters as in Fig. 3.

However, the photon envelope dependent bounds for decohering emitters are more accurate and can quantify the optimal duration (see Fig. 3).

To gain a better understanding of our results, we consider a pulse shape of the form

$$v(t) = \sum_{n=1}^{L} v_n \left[1 - \cos\left(\frac{2\pi n}{T}t\right)\right] \qquad (15)$$

for $0 < t < T$; otherwise, $v(t) = 0$. Pulses of this form are real $[v(t) \in \mathbb{R}]$, are symmetric, fulfill $v(0) = v(T) = \dot{v}(0) = \dot{v}(T) = 0$ [45], and contain L independent parameters T and v_n/v_1, with $n = 2, \dots, L$. For $L = 1$ this ansatz is a $\sin^2$ pulse with variable pulse duration. Using the basis of Eq. (15), normalization yields $v_1 = \sqrt{6/9T}$ $(L = 1)$, making it apparent that the only free parameter of the $\sin^2$ pulse is the duration.

We show the maximum worst-case fidelity $F(|\alpha_0| = 0)$ and average fidelity for $L = 1$ as a function of the pulse duration T in Fig. 3, confirming that the various approximate bounds fail to capture a useful bound for the maximum achievable fidelity for all possible timescales and fail to quantify the optimal duration, in contrast to the bound provided by Eq. (11) that does not rely on an adiabatic approximation and holds for any detuning.

The optimal duration balances the finite cavity coupling strength g and cavity decay rate κ with the decoherence of the emitter. We more thoroughly investigate the optimal duration for a $\sin^2$ pulse as a function of the qubit decoherence rates Γ_1 and Γ_2 in Fig. 5. For Fig. 5 we determine the optimal duration numerically in two steps. First, we find the optimal duration on a grid with 200 time points between $\max(1/g, 1/\kappa)$ and $\min(\Gamma_1, \Gamma_2)$ and then repeat the optimization with 200 additional points between the two points around the optimum of the first run. This approach ensures that even for small decoherence rates the grid is sufficiently small to avoid artifacts of the numerical grid. The decrease of the worst-case fidelity as well as the optimal duration as a function of the decoherence rates of the matter system becomes apparent in Fig. 5. However, the decrease of the duration flattens for higher rates as the duration is also limited from below due to the finite coupling between the matter qubit and the cavity
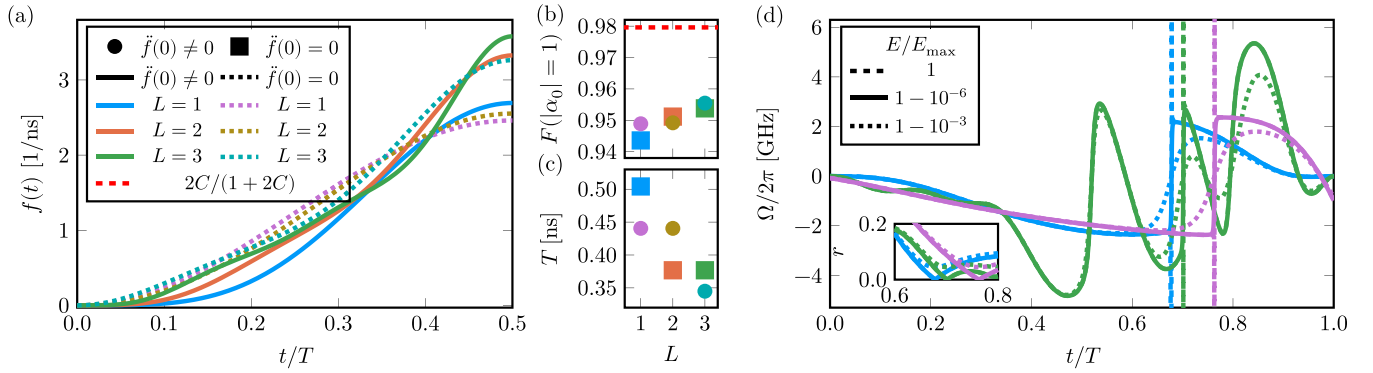
FIG. 6. Results of optimizing the pulse shape for a maximum worst-case fidelity. (a) shows half of the optimal symmetric pulse shapes $f(t)$ for different numbers of free parameters L and restrictions on the pulse (see legend). The corresponding worst-case fidelity $F(|\alpha_0| = 1)$ and optimal pulse duration T are depicted in (b) and (c); here. the dashed line corresponds to the perfect emitter bound [see Eq. (14)]. (d) Driving Rabi frequency $\Omega(t)$ as a function of time for different pulses [different colors; see the legend in (a)] and $E/E_{\max}$ (see legend). Reducing E leads to a larger minimal $|\alpha(t)| = e^{-\Gamma_2 t} r(t)$ (see inset) and smooths out discontinuities in $\Omega(t)$. Parameters are the same as in Fig. 3, $\Gamma_1, \Gamma_2 = 0.1\gamma$, and $\Delta = 0$. See Appendix E for the optimization results.

and the out-coupling rate of the cavity. Furthermore, we see that, qualitatively, the rates Γ_1 and Γ_2 behave similarly, but depending on the protocol of interest, it might be preferential to swap the roles of $|0\rangle$ and $|1\rangle$, i.e., couple the shorter- or longer-lived state to the excited state via the cavity.

C. Fidelity optimization by pulse shaping

More generally, we can take an ansatz for the envelope and optimize its independent parameters with regard to any quantity limited by Eq. (11). Here, we maximize the worst-case fidelity $F(|\alpha_0| = 1)$ [see Eq. (12)] to find $v_{opt} = \text{argmax}_v[1/\max_t e^{\Gamma_2 T} \int_0^t d(\tau)d\tau]$. The paradigm shift from searching for the optimal $\Omega(t)$ to searching the optimal pulse shape $v(t)$ (including the duration) saves one from repeatedly solving the dynamics and instead allows the use of the closed-form function $d(t)$ [Eq. (10)]; see Appendix D for the analytic evaluation of $\int_0^t d(\tau)d\tau$ for the ansatz in Eq. (15). Parametrizing $v(t)$ by $\vec{v}$, the optimization is over a finite parameter space instead of a function space, and the optimization assumes the well-known form of a (continuous) minimax problem [46,47] for finding the optimal $\vec{v}$. In Fig. 6 we show results for the ansatz in Eq. (15) and a grid optimization to find the L optimal parameters T and v_n/v_1 ($n = 2, \ldots, L$). It turns out that increasing L allows for higher fidelities and shorter pulses. We also display the photon shape and Rabi frequency, both of which we have immediate access to after the optimization. We remark that the optimization results can be confirmed using a single simulation of the Lindblad master equation with the optimal photon shape and Rabi frequency.

Constraints can be accounted for by different $v(t)$, e.g., by fixing some parameters; in particular, if the rate at which the drive can be modulated is larger than the optimal T, we can fix it to the minimal achievable T. In Fig. 6 we also show the optimization results ensuring a continuous drive activation by imposing $\ddot{v}(0) = 0$ [see Eqs. (7) and (8)]. To this end we use only odd n as free parameters and set $v_{2n} = -\frac{n^2}{(n+1)^2}v_{2n-1}$. Additionally, we show in Fig. 6(d) that targeting $E_{\max}$ leads

to a pole in the driving Rabi frequency $\Omega(t)$ (8) which can be avoided by smoothing $\Omega(t)$ by reducing the target efficiency $E < E_{\max}$.

V. CONCLUSION

In conclusion, we derived a bound for the fidelity for cavity-assisted stimulated Raman emission, taking into account not only the cavity quantum electrodynamic quantities but also the temporal pulse shape and additional decoherence processes of the three-level system. Due to the cascaded nature of the equations, we see great potential in applying the bounds to nontrivial waveguides. Furthermore, we showed how this bound can be cast into an optimization problem for the pulse shape for an efficient emission process, providing a paradigm shift from optimizing the drive to optimizing the temporal mode (and thereby also fixing the drive). We showed that this optimization is of a closed-form expression, in contrast to the naïve optimization, where the dynamics need to be solved (numerically) repeatedly. Combined with the encoding and entanglement protocols we proposed, this is a promising ingredient for quantum technology. The method of including the main emission process in the coherent dynamics by combining the novel input-output approach by [39,40] with the temporal mode matching can potentially be applied to many problems. While we grid optimized a symmetric pulse, nonsymmetric pulses compatible with the initial conditions, i.e., continuously vanishing at $t = 0$, and different optimization algorithms could be investigated analogously. A natural next step would be to study a photon-mediated matter-to-matter transfer within this framework.

ACKNOWLEDGMENTS

APPENDIX A: ROTATING FRAME AND LABORATORY FRAME

Since the main text introduces the Hamiltonian in the rotating frame, in this Appendix we link the rotating frame to the laboratory frame. The Hamiltonian in the laboratory frame is

$$\tilde{H}_S/\hbar = (\Delta + \omega_c) |e\rangle \langle e| - \delta |1\rangle \langle 1| + \omega_c c^\dagger c$$
$$+ [\tilde{\Omega}^*(t) |1\rangle \langle e| + g c^\dagger |0\rangle \langle e| + \text{H.c.}], \quad \text{(A1)}$$

with $\Delta + \omega_c$ being the excited state energy (in units of frequency), δ being the qubit level splitting, and ω_c being the cavity frequency. We then apply the transformation to the rotating frame

$$U = \exp[-i(-\delta |1\rangle \langle 1| + \omega_c |e\rangle \langle e| + \omega_c c^\dagger c)t], \quad \text{(A2)}$$

leading to

$$H_s/\hbar = U^\dagger \tilde{H}_S/\hbar U - i U^\dagger \dot{U}$$
$$= \Delta |e\rangle \langle e| + [\Omega^*(t) |1\rangle \langle e| + g c^\dagger |0\rangle \langle e| + \text{H.c.}], \quad \text{(A3)}$$

corresponding to the Hamiltonian in the main text. The detuning is Δ, and the drive in the laboratory frame is linked to the rotating frame by $\tilde{\Omega}(t) = \Omega(t) \exp[-i(\delta + \omega_c)t]$. Additionally, we see how the splitting between the qubit states is absorbed in the time-dependent drive.

Using the same transformation, we can also link the time dependence of the coupling to the virtual cavity $\tilde{g}_v(t) = g_v(t) e^{i\omega_c t}$ between the laboratory and rotating frames. This also links the photon envelopes $\tilde{v}(t) = e^{-i\omega_c t} v(t)$ and leads to the correct transformation of the dissipator L_0. Because the remaining dissipators gain only a global phase in the rotating frame and always occur in pairs (with their adjoint) in the master equation, we can treat the remaining dissipators as unchanged in the rotating frame.

APPENDIX B: DECOHERENCE RATES

In this Appendix we show how to derive the combined decoherence rates arising in the non-Hermitian Hamiltonian from established dissipators from the Lindblad master equation. The Lindblad master equation takes the form

$$\frac{d\rho}{dt} = -\frac{i}{\hbar}[H, \rho] + \sum_i \left(L_i \rho L_i^\dagger - \frac{1}{2}\{L_i^\dagger L_i, \rho\} \right), \quad \text{(B1)}$$

which is also found in the employed open quantum systems approach to input-output theory [39,40]. In addition to the main dissipator L_0 introduced in the main text we consider the following dissipators: (1) decays from the excited state (ES) $|e\rangle$ to the ground states (GSs) $|1\rangle$ and $|0\rangle$, $L_1 = \sqrt{\gamma} \cos(\xi) |1\rangle \langle e|$ and $L_2 = \sqrt{\gamma} \sin(\xi) |0\rangle \langle e|$, with ξ being the branching angle; (2) the important uncorrelated dephasing terms [48], here the dephasing of $|1\rangle$ and $|e\rangle$ using the phase of $|0\rangle$ as a reference, $L_3 = \sqrt{\Gamma_{\text{ph}}^1} |1\rangle \langle 1|$ and $L_4 = \sqrt{\Gamma_{\text{ph}}^e} |e\rangle \langle e|$; (3) incoherent transitions between the GSs, $L_5 = \sqrt{\Gamma_{0\to 1}} |1\rangle \langle 0|$ and $L_6 = \sqrt{\Gamma_{1\to 0}} |0\rangle \langle 1|$; and (4) unwanted cavity losses (e.g., losses through the wrong mirror), given by $L_7 = \sqrt{\tilde{\kappa}} c$.

The effect of these dissipators on the non-Hermitian Schrödinger equation

$$i\hbar \frac{\partial}{\partial t} |\Psi\rangle = H_{\text{NH}} |\Psi\rangle = \left(H - \hbar \frac{i}{2} \sum_i L_i^\dagger L_i \right) |\Psi\rangle \quad \text{(B2)}$$

depends only on $L_i^\dagger L_i$. This implies we can combine $\sum_{i=1,2,4} L_i^\dagger L_i = \tilde{\gamma} |e\rangle \langle e|$ with $\tilde{\gamma} = \gamma + \Gamma_{\text{ph}}^e$ and $\sum_{i=3,6} L_i^\dagger L_i = \Gamma_1 |1\rangle \langle 1|$ with $\Gamma_1 = \Gamma_{1\to 0} + \Gamma_{\text{ph}}^1$. In the main text we refer to $\Gamma_{0\to 1} = \Gamma_2$ for a consistent and simpler notation. Last, the cavity losses lead to $L_7^\dagger L_7 = \tilde{\kappa} c^\dagger c$.

APPENDIX C: SOLVING THE NON-HERMITIAN DYNAMICS

Combining the temporal mode matching and the non-Hermitian Schrödinger equation, the (decaying) dynamics of the coherent state transfer are

$$\dot{\alpha}(t) = -\frac{\Gamma_1}{2}\alpha(t) + \Omega^*(t)\zeta(t), \quad \dot{\beta}(t) = -\frac{\Gamma_2}{2}\beta(t), \quad \text{(C1)}$$

$$\dot{\zeta}(t) = \left(-i\Delta - \frac{\tilde{\gamma}}{2} \right)\zeta(t) - g\eta(t) - \Omega(t)\alpha(t), \quad \text{(C2)}$$

$$\dot{\eta}(t) = -\frac{\Gamma_2 + \kappa + \tilde{\kappa}}{2}\eta(t) + g\zeta(t), \quad \text{(C3)}$$

$$\dot{\lambda}(t) = -\frac{\Gamma_2}{2}\lambda(t) + \frac{\kappa|\eta(t)|^2}{2\lambda^*(t)}, \quad \text{(C4)}$$

where we combined important uncorrelated dephasing terms [48] and relevant decays from the states $|1\rangle$, $|0\rangle$, and $|e\rangle$ in the rates Γ_1, Γ_2, and $\tilde{\gamma}$, respectively.

To solve these equations we first formally integrate the pulse amplitude

$$\lambda(t) = \sqrt{\kappa} e^{i\varphi} \sqrt{\int_0^t e^{\Gamma_2(\tau - t)}|\eta(\tau)|^2 \, d\tau}, \quad \text{(C5)}$$

where we allow for an arbitrary initial phase φ. Inserting this solution into the temporal mode matching $g_v(t) = -\sqrt{\kappa}\eta^*(t)/\lambda^*(t)$ and comparing to the definition of the time-dependent coupling to the virtual cavity $g_v(t) = -v^*(t)/\sqrt{\int_0^t dt' |v(t')|^2}$ relates $\eta(t)$ to the pulse shape,

$$\eta(t) = E |\alpha_0| e^{i\varphi} e^{-\Gamma_2 t/2} v(t)/\sqrt{\kappa}, \quad \text{(C6)}$$

with $\alpha_0 = \alpha(0)$. We term the positive proportionality constant E the *matter-photon conversion efficiency* and demonstrated in the main text that it is directly related to the fidelity of the process. Equation (C6) shows that the pulse shape is directly linked to the dynamics of the ES, and combining Eqs. (C5) and (C6) with the temporal mode matching, we see that a static phase (such as φ) can be encoded in either $\lambda(t)$ and or $v(t)$. Reinserting $\eta(t)$ into the formal integral describing the photon probability amplitude yields

$$\lambda(t) = E |\alpha_0| e^{i\varphi - \Gamma_2 t/2} \sqrt{\int_0^t |v(\tau)|^2 \, d\tau}. \quad \text{(C7)}$$

Inspired by results for the optimal control to emit a photon of a certain shape [31], we solve the remaining equations *in*

reverse by imposing a fixed photon shape [and thereby $\eta(t)$ and $\lambda(t)$]. This approach leads us to

$$\zeta(t) = \frac{\Gamma_2 + \kappa + \tilde{\kappa}}{2g}\eta(t) + \frac{1}{g}\dot{\eta}(t), \qquad (C8)$$

and the optimal drive

$$\Omega(t) = -\frac{(\tilde{\gamma}/2 + i\Delta)\zeta(t) + g\eta(t) + \dot{\zeta}(t)}{\alpha(t)}. \qquad (C9)$$

Because we can ensure that $|\alpha(t)| > 0$ for $0 \leqslant t < T$ if $\alpha_0 \neq 0$ and the form of $\Omega(t)$ is irrelevant for $\alpha_0 = 0$ as no emission takes place, this provides a solution of Eq. (C2) for $\Omega(t)$. Additionally, we now choose φ such that $\Omega(t)$ becomes independent of the initial condition, i.e., $|\alpha_0| e^{i\varphi} = \alpha_0$,

implying that the phase of α_0 becomes the phase of $\lambda(t)$. The complex phase of $\Omega(t)$ is then determined by only the system parameters and the pulse shape $v(t)$, not the initial condition of the matter qubit.

To separate Eq. (C1) into two separable (in t) real equations we take the ansatz $\alpha(t) = \alpha_0 r(t) e^{i\phi(t) - \Gamma_1 t/2}$, with $r(t), \phi(t) \in \mathbb{R}$, $r(0) = 1$, and $\phi(0) = 0$. The separation yields $r\dot{r} = -\frac{1}{2}E^2 d(t)$ with the depletion rate according to Eq. (10) of the main text. We can integrate both sides of the separated equation for $\dot{r}$ to calculate the solution used in the main text for $r^2(t) = 1 - E^2 \int_0^t d(\tau)d\tau \geqslant 0$. Note that $r(t)$ and $d(t)$ are independent of the detuning Δ.

After this integral is solved, the phase evolution also becomes a straightforward integral, i.e.,

$$\phi(t) = \int_0^t \frac{F^2 e^{(\Gamma_1 - \Gamma_2)t}}{g^2 r^2(t)} \left\{ \left[\left(1 + \frac{\tilde{\kappa}}{\kappa}\right)(\Delta + \dot{\theta}(t)) + \frac{\ddot{\theta}(t)}{\kappa} \right] f(t)\dot{f}(t) + \frac{\Delta + 2\dot{\theta}(t)}{\kappa}\dot{f}^2(t) - \frac{\dot{\theta}(t)}{\kappa}f(t)\ddot{f}(t) \right.$$

$$\left. + \left[\frac{\kappa}{4}\left(1 + \frac{\tilde{\kappa}}{\kappa}\right)^2(\Delta + \dot{\theta}(t)) + \left(1 + \frac{\tilde{\kappa}}{\kappa}\right)\frac{\ddot{\theta}(t)}{2} + \frac{1}{\kappa}\left(\Delta\dot{\theta}^2(t) - g^2\dot{\theta}(t) + \dot{\theta}^3(t)\right) \right] f^2(t) \right\} dt, \qquad (C10)$$

where $\theta(t) \in \mathbb{R}$ is the photon envelope phase and $f(t) \in \mathbb{R}$ is the amplitude, i.e., $v(t) = e^{i\theta(t)}f(t)$. We can read off from this expression that $\phi(t) = \phi(0) = 0$ for $\Delta = 0$ and $\dot{\theta}(t) = 0$, implying that the phase ϕ is constant for $\Delta = 0$ and $\dot{\theta}(t) = 0$, i.e., a resonant cavity and a pulse shape with a constant complex argument.

APPENDIX D: ANALYTIC SOLUTION OF THE INTEGRATED DEPLETION RATE

In this Appendix we show the analytic expression for $G(t) = \int_0^t d(\tau)d\tau$ for the real pulse shape introduced in the main text, given by

$$v(t) = f(t) = \sum_{n=1}^L v_n \left[1 - \cos\left(\frac{2\pi n}{T}t\right)\right] = \sum_{n=1}^L v_n f_n(t). \qquad (D1)$$

Because this pulse shape is real, we can write

$$G(t) = \int_0^t e^{t(\Gamma_1 - \Gamma_2)} \left\{ \left[1 + \frac{\tilde{\kappa}}{\kappa} + \frac{\tilde{\gamma} - \Gamma_2}{g^2}\frac{\kappa}{4}\left(1 + \frac{\tilde{\kappa}}{\kappa}\right)^2 \right] f^2(t) + \left[\frac{1}{g^2}\left(1 + \frac{\tilde{\kappa}}{\kappa}\right) + \frac{\tilde{\gamma} - \Gamma_2}{\kappa g^2} \right] \dot{f}^2(t) \right.$$

$$\left. + \left[\frac{2}{\kappa} + \frac{\kappa}{2g^2}\left(1 + \frac{\tilde{\kappa}}{\kappa}\right)^2 + \frac{\tilde{\gamma} - \Gamma_2}{g^2}\left(1 + \frac{\tilde{\kappa}}{\kappa}\right) \right] f(t)\dot{f}(t) + \frac{1}{g^2}\left(1 + \frac{\tilde{\kappa}}{\kappa}\right)f(t)\ddot{f}(t) + \frac{2}{\kappa g^2}\dot{f}(t)\ddot{f}(t) \right\} dt, \qquad (D2)$$

where using the ansatz (D1) enables us to integrate termwise. This means the full integral takes the form $\sum_{n,m} v_n v_m X$, where X is made up from products of the prefactor and the integrals shown below. For brevity of notation we use $\Gamma = \Gamma_1 - \Gamma_2$ and $\omega_n = \frac{2\pi n}{T}$ to write the different terms for the integral

$$\int_0^t e^{\Gamma t} f_n(t)f_m(t)dt = \begin{cases} \frac{u_{m-n}(t, \Gamma) + u_{m+n}(t, \Gamma)}{2} + \frac{e^{\Gamma t} - 1}{\Gamma} - u_n(t, \Gamma) - u_m(t, \Gamma) \text{ for } \Gamma \neq 0, \\ \frac{3t}{2} + \frac{\sin(2\omega_m t)}{4\omega_m} - 2\frac{\sin(\omega_m t)}{\omega_m} \text{ for } \Gamma = 0 \text{ and } n = m, \\ \frac{u_{m-n}(t, \Gamma=0) + u_{m+n}(t, \Gamma=0)}{2} - u_n(t, \Gamma=0) - u_m(t, \Gamma=0) + t \text{ else,} \end{cases} \qquad (D3)$$

$$\int_0^t e^{\Gamma t} f_n(t)\dot{f}_m(t)dt = \omega_m \begin{cases} \frac{1 - \cos(\omega_m t)}{\omega_m} - \frac{1 - \cos(\omega_{2m} t)}{2\omega_{2m}} \text{ for } \Gamma = 0 \text{ and } n = m, \\ u_m(t) + \frac{u_{m+n}(t, \Gamma) + u_{m-n}(t, \Gamma)}{2} \text{ else,} \end{cases} \qquad (D4)$$

$$\int_0^t e^{\Gamma t} \dot{f}_n(t)\dot{f}_m(t)dt = \frac{1}{2}\omega_n\omega_m \begin{cases} t - \frac{\sin(2\omega_m t)}{2\omega_m} \text{ for } \Gamma = 0 \text{ and } n = m, \\ h_{m+n}(t, \Gamma) - h_{m+n}(t, \Gamma) \text{ else,} \end{cases} \qquad (D5)$$

$$\int_0^t e^{\Gamma t} f_n(t)\ddot{f}_m(t)dt = \frac{1}{2}\omega_m^2 \begin{cases} 2h_m(t, \Gamma=0) - t + \frac{\sin(2\omega_m t)}{2\omega_m} \text{ for } \Gamma = 0 \text{ and } n = m, \\ 2h_m(t, \Gamma) - h_{m+n}(t, \Gamma) - h_{m+n}(t, \Gamma) \text{ else,} \end{cases} \qquad (D6)$$

TABLE I. Optimized pulse parameters. The durations are rounded to two (three for $E_{\max}$) decimal digits. The duration T is given in nanoseconds, and the amplitudes are given in units of 1/ns.

L	$\ddot{f}(0) = 0$	$E_{\max}$	T	v_1	v_2	v_3	v_4	v_5	v_6
1	yes	0.987	0.50	1.35	-0.34				
2	yes	0.987	0.38	1.5	-0.38	0.16	-0.09		
3	yes	0.988	0.38	1.44	-0.36	0.27	-0.15	0.08	-0.06
1	no	0.988	0.44	1.23					
2	no	0.988	0.44	1.28	-0.07				
3	no	0.988	0.34	1.46	-0.30	0.17			

$$\int_0^t e^{\Gamma t} \dot{f}_n(t) \ddot{f}_m(t) dt = \frac{1}{2} \omega_n \omega_m^2 \begin{cases} \frac{1 - \cos(\omega_{2m} t)}{\omega_{2m}} & \text{for } \Gamma = 0 \text{ and } n = m, \\ u_{m+n}(t, \Gamma) - u_{m+n}(t, \Gamma) & \text{else,} \end{cases} \tag{D7}$$

with

$$h_m(t, \Gamma) = \frac{1}{\Gamma^2 + \omega_m^2} \{ e^{\Gamma t} [\omega_m \sin(\omega_m t) + \Gamma \cos(\omega_m t)] - \Gamma \}, \tag{D8}$$

$$u_m(t, \Gamma) = \frac{1}{\Gamma^2 + \omega_m^2} \{ \omega_m + e^{\Gamma t} [\Gamma \sin(\omega_m t) - \omega_m \cos(\omega_m t)] \}. \tag{D9}$$

APPENDIX E: OPTIMIZED PULSE SHAPES

To optimize the pulse shapes in Fig. 3 we use 500 samples for T between $\max(1/\kappa, 1/g)$ and $\min(1/\Gamma_1, 1/\Gamma_2)$ (here, ≈ 0.03 and 16 ns) and, for each λ_n/λ_1 ($n = 2, \ldots, L$), 200 samples between -1 and 1. With this we can numerically determine the maxima of these discrete points. Table I shows the optimization results of Fig. 3 in the main text.

[1] J. I. Cirac, P. Zoller, H. J. Kimble, and H. Mabuchi, Quantum state transfer and entanglement distribution among distant nodes in a quantum network, Phys. Rev. Lett. **78**, 3221 (1997).

[2] T. van Leent, M. Bock, F. Fertig, R. Garthoff, S. Eppelt, Y. Zhou, P. Malik, M. Seubert, T. Bauer, W. Rosenfeld, W. Zhang, C. Becher, and H. Weinfurter, Entangling single atoms over 33 km telecom fibre, Nature (London) **607**, 69 (2022).

[3] N. Gisin and R. Thew, Quantum communication, Nat. Photonics **1**, 165 (2007).

[4] K. Nemoto, M. Trupke, S. J. Devitt, A. M. Stephens, B. Scharfenberger, K. Buczak, T. Nöbauer, M. S. Everitt, J. Schmiedmayer, and W. J. Munro, Photonic architecture for scalable quantum information processing in diamond, Phys. Rev. X **4**, 031022 (2014).

[5] W. J. Munro, K. Azuma, K. Tamaki, and K. Nemoto, Inside quantum repeaters, IEEE J. Sel. Top. Quantum Electron. **21**, 78 (2015).

[6] F. Grasselli, H. Kampermann, and D. Bruß, Conference key agreement with single-photon interference, New J. Phys. **21**, 123002 (2019).

[7] W. Zhang, T. van Leent, K. Redeker, R. Garthoff, R. Schwonnek, F. Fertig, S. Eppelt, W. Rosenfeld, V. Scarani, C. C.-W. Lim, and H. Weinfurter, A device-independent quantum key distribution system for distant users, Nature (London) **607**, 687 (2022).

[8] D. P. Nadlinger, P. Drmota, B. C. Nichol, G. Araneda, D. Main, R. Srinivas, D. M. Lucas, C. J. Ballance, K. Ivanov, E. Y.-Z. Tan, P. Sekatski, R. L. Urbanke, R. Renner, N. Sangouard, and J.-D. Bancal, Experimental quantum key distribution certified by Bell's theorem, Nature (London) **607**, 682 (2022).

[9] H. J. Kimble, The quantum internet, Nature (London) **453**, 1023 (2008).

[10] S. Wehner, D. Elkouss, and R. Hanson, Quantum internet: A vision for the road ahead, Science **362**, eaam9288 (2018).

[11] J. L. O'Brien, A. Furusawa, and J. Vučković, Photonic quantum technologies, Nat. Photonics **3**, 687 (2009).

[12] V. Giovannetti, S. Lloyd, and L. Maccone, Advances in quantum metrology, Nat. Photonics **5**, 222 (2011).

[13] A. Aspuru-Guzik and P. Walther, Photonic quantum simulators, Nat. Phys. **8**, 285 (2012).

[14] S. Slussarenko and G. J. Pryde, Photonic quantum information processing: A concise review, Appl. Phys. Rev. **6**, 041303 (2019).

[15] D. J. Brod, E. F. Galvão, A. Crespi, R. Osellame, N. Spagnolo, and F. Sciarrino, Photonic implementation of boson sampling: A review, Adv. Photonics **1**, 034001 (2019).

[16] C. D. Bruzewicz, J. Chiaverini, R. McConnell, and J. M. Sage, Trapped-ion quantum computing: Progress and challenges, Appl. Phys. Rev. **6**, 021314 (2019).

[17] G. Burkard, T. D. Ladd, A. Pan, J. M. Nichol, and J. R. Petta, Semiconductor spin qubits, Rev. Mod. Phys. **95**, 025003 (2023).

[18] M. Kjaergaard, M. E. Schwartz, J. Braumüller, P. Krantz, J. I.-J. Wang, S. Gustavsson, and W. D. Oliver, Superconducting qubits: Current state of play, Annu. Rev. Condens. Matter Phys. **11**, 369 (2020).

[19] C. H. Bennett and G. Brassard, Quantum cryptography: Public key distribution and coin tossing, Theor. Comput. Sci. **560**, 7 (2014), reprinted from a 1984 paper.

[20] A. Kuhn, M. Hennrich, and G. Rempe, Deterministic single-photon source for distributed quantum networking, Phys. Rev. Lett. **89**, 067901 (2002).

[21] L.-M. Duan, A. Kuzmich, and H. J. Kimble, Cavity QED and quantum-information processing with "hot" trapped atoms, Phys. Rev. A **67**, 032305 (2003).

[22] O. Morin, M. Körber, S. Langenfeld, and G. Rempe, Deterministic shaping and reshaping of single-photon temporal wave functions, Phys. Rev. Lett. **123**, 133602 (2019).

[23] P. B. R. Nisbet-Jones, J. Dilley, D. Ljunggren, and A. Kuhn, Highly efficient source for indistinguishable single photons of controlled shape, New J. Phys. **13**, 103036 (2011).

[24] T. M. Sweeney, S. G. Carter, A. S. Bracker, M. Kim, C. S. Kim, L. Yang, P. M. Vora, P. G. Brereton, E. R. Cleveland, and D. Gammon, Cavity-stimulated Raman emission from a single quantum dot spin, Nat. Photonics **8**, 442 (2014).

[25] B. C. Pursley, S. G. Carter, M. K. Yakes, A. S. Bracker, and D. Gammon, Picosecond pulse shaping of single photons using quantum dots, Nat. Commun. **9**, 115 (2018).

[26] S. Sun, J. L. Zhang, K. A. Fischer, M. J. Burek, C. Dory, K. G. Lagoudakis, Y.-K. Tzeng, M. Radulaski, Y. Kelaita, A. Safavi-Naeini, Z.-X. Shen, N. A. Melosh, S. Chu, M. Lončar, and J. Vučković, Cavity-enhanced Raman emission from a single color center in a solid, Phys. Rev. Lett. **121**, 083601 (2018).

[27] E. N. Knall, C. M. Knaut, R. Bekenstein, D. R. Assumpcao, P. L. Stroganov, W. Gong, Y. Q. Huan, P.-J. Stas, B. Machielse, M. Chalupnik, D. Levonian, A. Suleymanzade, R. Riedinger, H. Park, M. Lončar, M. K. Bhaskar, and M. D. Lukin, Efficient source of shaped single photons based on an integrated diamond nanophotonic system, Phys. Rev. Lett. **129**, 053603 (2022).

[28] C. K. Law and H. J. Kimble, Deterministic generation of a bitstream of single-photon pulses, J. Mod. Opt. **44**, 2067 (1997).

[29] A. V. Gorshkov, A. André, M. D. Lukin, and A. S. Sørensen, Photon storage in Λ-type optically dense atomic media. I. Cavity model, Phys. Rev. A **76**, 033804 (2007).

[30] J. Dilley, P. Nisbet-Jones, B. W. Shore, and A. Kuhn, Single-photon absorption in coupled atom-cavity systems, Phys. Rev. A **85**, 023834 (2012).

[31] G. S. Vasilev, D. Ljunggren, and A. Kuhn, Single photons made-to-measure, New J. Phys. **12**, 063024 (2010).

[32] M. Khanbekyan and D.-G. Welsch, Cavity-assisted spontaneous emission of a single Λ-type emitter as a source of single-photon packets with controlled shape, Phys. Rev. A **95**, 013803 (2017).

[33] M. Mücke, J. Bochmann, C. Hahn, A. Neuzner, C. Nölleke, A. Reiserer, G. Rempe, and S. Ritter, Generation of single photons from an atom-cavity system, Phys. Rev. A **87**, 063805 (2013).

[34] A. Baksic, R. Belyansky, H. Ribeiro, and A. A. Clerk, Shortcuts to adiabaticity in the presence of a continuum: Applications to itinerant quantum state transfer, Phys. Rev. A **96**, 021801(R) (2017).

[35] P.-J. Stas, Y. Q. Huan, B. Machielse, E. N. Knall, A. Suleymanzade, B. Pingault, M. Sutula, S. W. Ding, C. M. Knaut, D. R. Assumpcao, Y.-C. Wei, M. K. Bhaskar, R. Riedinger, D. D. Sukachev, H. Park, M. Lončar, D. S. Levonian, and M. D. Lukin, Robust multi-qubit quantum network node with integrated error detection, Science **378**, 557 (2022).

[36] S. D. Barrett and P. Kok, Efficient high-fidelity quantum computation using matter qubits and linear optics, Phys. Rev. A **71**, 060310(R) (2005).

[37] L. Giannelli, T. Schmit, T. Calarco, C. P. Koch, S. Ritter, and G. Morigi, Optimal storage of a single photon by a single intracavity atom, New J. Phys. **20**, 105009 (2018).

[38] N. H. Lindner and T. Rudolph, Proposal for pulsed on-demand sources of photonic cluster state strings, Phys. Rev. Lett. **103**, 113602 (2009).

[39] A. H. Kiilerich and K. Mølmer, Input-output theory with quantum pulses, Phys. Rev. Lett. **123**, 123604 (2019).

[40] A. H. Kiilerich and K. Mølmer, Quantum interactions with pulses of radiation, Phys. Rev. A **102**, 023717 (2020).

[41] J. Dalibard, Y. Castin, and K. Mølmer, Wave-function approach to dissipative processes in quantum optics, Phys. Rev. Lett. **68**, 580 (1992).

[42] K. Mølmer, Y. Castin, and J. Dalibard, Monte Carlo wave-function method in quantum optics, J. Opt. Soc. Am. B **10**, 524 (1993).

[43] H. J. Carmichael, Quantum trajectory theory for cascaded open systems, Phys. Rev. Lett. **70**, 2273 (1993).

[44] A. J. Daley, Quantum trajectories and open many-body quantum systems, Adv. Phys. **63**, 77 (2014).

[45] J. M. Martinis and M. R. Geller, Fast adiabatic qubit gates using only σ_z control, Phys. Rev. A **90**, 022307 (2014).

[46] B. Rustem and M. Howe, An approach to continuous minimax: The basic algorithm, IFAC Proc. **31**, 429 (1998).

[47] B. Rustem and M. Howe, *Algorithms for Worst-Case Design and Applications to Risk Management* (Princeton University Press, Princeton, NJ, 2009).

[48] J. Li, M. A. Sillanpää, G. S. Paraoanu, and P. J. Hakonen, Pure dephasing in a superconducting three-level system, J. Phys.: Conf. Ser. **400**, 042039 (2012).